

Applied Catalysis B: Environmental

Improved photocatalytic hydrogen evolution over porous carbon nitride nanosheets by introducing carbon and nitrogen double vacancies --Manuscript Draft--

Manuscript Number:	APCATB-D-20-05657
Article Type:	Research Paper
Section/Category:	Photocatalysis and Photoelectrocatalysis
Keywords:	carbon nitride; carbon vacancies; double vacancies; porous structure; photocatalytic hydrogen evolution
Corresponding Author:	Huihui Li Lanzhou University Lanzhou, CHINA
First Author:	Huihui Li
Order of Authors:	Huihui Li Fuchun Ning Xiaofei Chen Anye Shi
Abstract:	<p>Porous carbon nitride nanosheets with carbon and nitrogen double vacancies have been synthesized by soft template-supported one-pot method. Besides a highly defined and unambiguous structure, it also shows minimal thickness nanosheets and high crystallinity. This porous carbon nitride exhibits the greatly enhanced photocatalytic hydrogen generation activity under visible light ($297.6 \mu\text{mol h}^{-1}$), which is 9.6 times higher than $31.2 \mu\text{mol h}^{-1}$ of pristine one. The apparent quantum yield of 12.7 % at 420 nm for hydrogen production can be achieved over this porous nanosheets. The detail investigation suggests that there are carbon vacancies along with nitrogen vacancies. Besides nitrogen vacancies, carbon vacancies also play a positive role on the improvement of hydrogen evolution. In addition, the photocatalytic performance especially hydrogen evolution is growing with the increase of C/N ratio.</p>



Lanzhou
28th October 2020

Dear *Appl. Catal. B* editors,

On behalf of all authors, I am delighted to submit a manuscript entitled “**Improved photocatalytic hydrogen evolution over porous carbon nitride nanosheets by introducing carbon and nitrogen double vacancies**” to your appreciation and to the editorial analysis of the *Appl. Catal. B* as to the possibility of its publication.

This manuscript is based on the synergistic effect of carbon and nitrogen vacancies in porous carbon nitride nanosheets for enhanced photocatalytic hydrogen evolution.

In this paper, the porous carbon nitride nanosheets with large size but no more than three atomic layers was prepared by a soft template assisted one-pot thermal process. Porous structure, carbon and nitrogen vacancies are simultaneously introduced into the framework of carbon nitride by a simple co-pyrolysis of melamine and polyvinyl pyrrolidone (PVP). By regulating the usage amount of PVP and controlling the thermal annealing time, a proper porous structure with proper carbon and nitrogen vacancies are generated. The synergetic effect of the carbon and nitrogen vacancies leads to the change of band structure and charge carriers, causing the change of electron transition. The transitions from impurity levels play a key role in excitation process, which improve the charge separation significantly. Such carbon nitride exhibits excellent photocatalytic hydrogen evolution activity (297.6 $\mu\text{mol h}^{-1}$, 100 mg of photocatalyst) under white LED lamp irradiation, which is almost 9.6 times higher than pristine carbon nitride because of the improved efficiency of charge separation and specific porous structure. In addition, the photocatalytic hydrogen evolution activity increases with increasing the carbon to nitrogen atomic ratio in carbon nitride. We believe this manuscript is valuable for all the researchers who are interested in photocatalytic water splitting for hydrogen evolution over carbon nitride.

The manuscript has not been published before and is not being considered for publication elsewhere. All authors have contributed to the creation of this manuscript for important intellectual content and read and approved the final manuscript. We declare there is no conflict of interest.

Thanks for your time and consideration.

Yours Sincerely,

Huihui Li

Corresponding author: Ph.D. Huihui Li

Address: Lanzhou University, 222 South Tianshui Road, Lanzhou 730000, China

Email: lihh@lzu.edu.cn

Please consider, as potential referees,

1) Lihua Lin

E-mail: lhlin@shinshu-u.ac.jp

2) Shanshan Chen

Email: s_chen@shinshu-u.ac.jp

3) Yongfa Zhu

E-mail: zhuyf@mail.tsinghua.edu.cn

Improved photocatalytic hydrogen evolution over porous carbon nitride nanosheets by introducing carbon and nitrogen double vacancies

Huihui Li ^{*1}, Fuchun Ning¹, Xiaofei Chen, Anye Shi

National & Local Joint Engineering Laboratory for Optical Conversion Materials and Technology, Key Laboratory of Special Function Materials and Structure Design, Ministry of Education, Lanzhou University, 222 South Tianshui Road, Lanzhou 730000, China

*Corresponding author: lihh@lzu.edu.cn

¹These authors are co-first authors.

Abstract: Porous carbon nitride nanosheets with carbon and nitrogen double vacancies have been synthesized by soft template-supported one-pot method. Besides a highly defined and unambiguous structure, it also shows minimal thickness nanosheets and high crystallinity. This porous carbon nitride exhibits the greatly enhanced photocatalytic hydrogen generation activity under visible light ($297.6 \mu\text{mol h}^{-1}$), which is 9.6 times higher than $31.2 \mu\text{mol h}^{-1}$ of pristine one. The apparent quantum yield of 12.7 % at 420 nm for hydrogen production can be achieved over this porous nanosheets. The detail investigation suggests that there are carbon vacancies along with nitrogen vacancies. Besides nitrogen vacancies, carbon vacancies also play a positive role on the improvement of hydrogen evolution. In addition, the photocatalytic performance especially hydrogen evolution is growing with the increase of C/N ratio.

Key words: carbon nitride; carbon vacancies; double vacancies; porous 2D structure; photocatalytic hydrogen evolution

1. Introduction

Developing semiconductor photocatalyst is a promising strategy to realize solar water splitting for hydrogen evolution [1]. As a metal-free semiconductor photocatalyst, carbon nitride is one of the suitable candidates as a visible-light response photocatalyst for H₂ production, since it possesses a narrow bandgap and proper conduction band potential for water reduction [2]. However, carbon nitride photocatalyst suffers from small surface area, low crystallinity and high electron-hole recombination rates [3]. Tremendous attempts have been made to boost its performance, including construction of heterostructure, design of porous structure, modification of electronic structure by heteroatoms doping or metal coordination and grafting functional group [4-8].

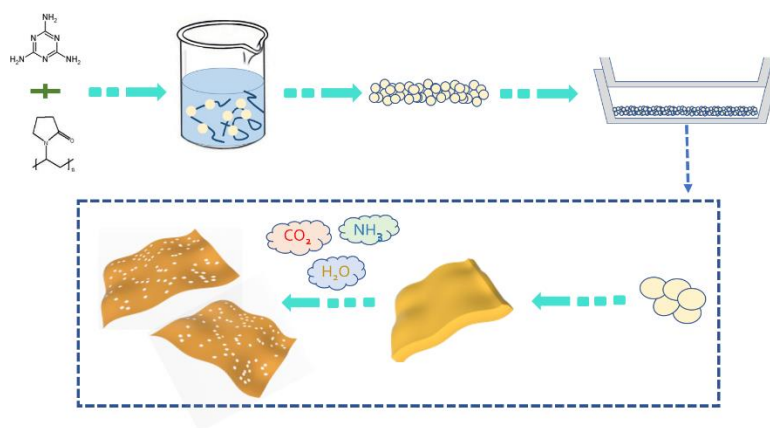
Among various modifications, the design of porous structure is considered to be an efficient way to improve the photocatalytic performance of carbon nitride by providing abundant active sites and decrease charge diffusion distance [9,10]. Particularly, the defect modification can be carried out in the process of porous structure formation [11]. On one hand, the formed nitrogen vacancies can modify the electronic structure in the porous carbon nitride. Zhang et. al reported that nitrogen vacancies were generated in a rapid high-temperature prepared porous carbon nitride, resulting in a more negative VBM, a more negative CBM, and a blue-shift absorption edge [12]. Ruan et. al reported that an increase of urea in the mixture precursor of melamine and urea led to an increase of nitrogen vacancies acting as trap states in mesoporous carbon nitride [13]. Porous carbon nitride via thermal polymerization of a freeze-dried crystalline mixture containing dicyandiamide and ammonium chloride under nitrogen atmosphere had

nitrogen vacancies resulting in the negative shift of potential of CB and forming defect states below CB acting as intermediate energy levels [14]. The introduction of controlled defects is regarded as an efficient way to modify the band structure with the generation of new trap states, perform as active sites and participate in the catalytic reaction directly [15]. On the other hand, the effect of carbon vacancies on the performance of carbon nitride also attracts researchers' attention. Liang et. al reported that the downshift of CB and VB and the blue-shift of absorption edge in the NH_3 -treated carbon nitride with carbon vacancies [16]. The photo-generated electrons can be trapped by carbon vacancies and then to produce relevant active species in carbon nitride nanotube [17]. After NH_3 etching thermal treatment, the H_2 evolution activity over carbon nitride was improved owing to the formation of carbon vacancies and porous structure [18]. Moreover, the presence of carbon vacancies can improve the photocatalytic H_2O_2 generation over carbon nitride [19].

In addition, the double nitrogen vacancies also have a benefit for the enhanced photocatalytic performance of carbon nitride, i.e. the NH_x and $\text{N}_{2\text{C}}$ vacancies, two types of N vacancies, introduced into the framework of polymeric carbon nitride will enhance the efficiency in hydrogen peroxide generation [20]. It is also believed that double vacancies of carbon and nitrogen in the carbon nitride may cause the redistribution of charge densities and thus activate adjacent C and N atoms for catalysis [21]. Introducing carbon and nitrogen vacancies simultaneously into carbon nitride will enhance visible light absorption and an extended charge carrier lifetime [22]. However, the double heterogeneous vacancies modification in carbon nitride is still characterized by

significant challenges for photocatalytic hydrogen evolution.

Herein, the porous carbon nitride photocatalyst with double heterogeneous vacancies was synthesized using melamine as a precursor and polyvinyl pyrrolidone (PVP) as a soft template. As depicted in Scheme 1, the uniform mixture of the melamine and PVP was heated in a crucible boat covered with another crucible boat like a mini atmosphere furnace [23]. After investigated the influence of template content and heating period as shown in Fig. S1-S5, the porous carbon nitride with double heterogeneous vacancies was obtained with an optimal preparation condition. The photocatalytic hydrogen evolution reaction over the as-fabricated porous structured photocatalyst was performed under white LED lamp irradiation. The relationship between porous structure with double heterogeneous vacancies and photocatalytic activity is investigated based on the various characterization results.



Scheme 1. An illustration of the preparation of porous CN-PVP photocatalyst.

2. Experimental

All the chemicals were purchased from Aladdin Chemical Reagent Co. Ltd. and used without further purification.

2.1. Samples preparation

Typically, 10 g of melamine and 500 mL of PVP aqueous solution with different concentration (2~100 g/L) were dispersed under vigorous stirring for 6 h. After centrifugation, the mixture was dried at 80 °C overnight. Then, the final powder was obtained after calcined at 550 °C with a heating rate of 5 °C min⁻¹ for different time (x=1, 2, 3, 4, 6, and 8 h) in air, which was denoted as CN-PVP. For comparison, bulk carbon nitride was synthesized by directly heating melamine under the same conditions and labelled as BCN.

2.2. Characterization

X-ray diffraction(XRD)characterizations were performed through the Bruker D2 PHASER powder X-ray diffractometer with graphite monochromator using Cu K α radiation (λ = 1.54184 Å). Fourier transform infrared (FT-IR) spectra were recorded using a VERTEX 70 V/80 V spectrometer (Bruker, Germany) by means of the K Br pellet technique. The UV–vis diffuse reflectance spectra (DRS) were obtained on a Perkin-Elmer Lambda 950 spectrometer equipped with Labsphere integrating over the spectral range of 300-800 nm and with BaSO₄ as reflectance standard. X-ray photoelectron spectroscopy (XPS) measurement was done using a XPS system (XPS, PHI-5702, Physical Electronics) with a monochromatic Al K source and a charge neutralizer, all the binding energies were referenced to the C1s peak at 284.6 eV of the

surface adventitious carbon. Atomic force microscopy (AFM) study in the present work was performed by Agilent 5500 ILM. The specific surface areas were measured out by the BET method (Micromeritics Instruments, TriStar α 3020). Photoluminescence (PL) spectra measurements were performed using a FLS-920 T fluorescence spectrophotometer with the excitation wavelength of 365 nm. The luminescence decay curves gained by FLS-920T fluorescence spectrophotometer with nF900 nanosecond flash lamp. Moreover, the transmission electron microscopy (TEM) is tested via the F30 S-TWIN electron microscopy (Tecnai G2, FEI Company). Electron spinning resonance (ESR) was measured by JES-FA300. Mott-Schottky plots were obtained by an electrochemical work-station (CHI 660E).

2.3. Photocatalytic performance

2.3.1. Light source

- (a) white light LED lamp (365~940 nm) with the intensity of 100 mW cm⁻²;
- (b) a series of monochromatic LED lamp with the same intensity of 10 mW cm⁻²;
- (c) 300 W Xenon (>420 nm) with the intensity of 165 mW cm⁻².

2.3.2. Photocatalytic H₂ evolution

Photocatalytic hydrogen evolution was carried out in a closed Pyrex top-irradiation vessel (150 mL). Typically, 100 mg of catalyst was dispersed in a 100 mL of triethylamine (TEOA, 10 vol.%) aqueous solution. Cocatalyst (1 wt.% Pt) was introduced by photodeposition. Prior to irradiation, the reaction solution sealed with a silicon stopper was purged by dry nitrogen blowing for 1 h to remove air. A 250 μ L gas-microsyringe was used to extract 100 μ L of evolved gas for testing. A calibrated Varian

GC-3380 Gas Chromatograph equipped with a thermal conductivity detector and a 5 Å molecular sieve column was employed to analyze the evolved gas, using argon gas as the carrier gas.

The apparent quantum yield (AQY) for the H₂ evolution was measured using the same experimental setup under different monochromatic LED lamp irradiation (10 mW cm⁻², 12.6 cm²). The AQY was calculated as $AQY = Ne/Np \times 100\%$, where Ne is the amount of reaction electrons, Np is the amount of incident photons [24].

2.3.3. Degradation experiments of dyes solution

The photocatalytic activities of samples were also evaluated by degrading different dyes aqueous solutions. Typically, 30 mg of photocatalyst was dispersed in 50 mL of different dyes aqueous solution (10 mg L⁻¹) and magnetically stirred in the dark. After 30 min to ensure an adsorption-desorption equilibrium, a white LED lamp was employed as irradiation source. Then, 3 mL of suspensions were collected for analysis at given time intervals. After centrifugation, the dye concentration was monitored. The target dyes including methyl orange (MO), methylene blue (MB), rhodamine B (RhB) and phenol were degraded.

2.4. Photoelectrochemical measurements

Photocurrent measurements were carried out on an electrochemical workstation (CS 310, Wuhan Corrtest Instrument Co. Ltd.) in a standard three electrode system, with the as-prepared samples (effective area is 1 cm²) as working electrodes, a platinum foil as the counter electrode and an Ag/AgCl (saturated KCl) electrode as a reference electrode. The working electrodes were suspended into Na₂SO₄ (0.1 mol L⁻¹) aqueous

solution with a 300 W Xe arc lamp equipped with a UVIRCUT filter (420 nm) regarded as the visible light source. All measurements are carried out with light ON-OFF switches of 6 s at a constant potential of 0.1 V to the working electrode. The electrochemical impedance spectroscopies (EIS) are performed at the open circuit potential. The frequency is ranging from 0.01 Hz to 100,000 Hz and the amplitude of the sinusoidal wave is 10 mV.

2.5. Ninhydrin test

Similar to a literature, 1 mL of ninhydrin ethanol solution (5 mg mL⁻¹) was added to 5 mL of sample suspension (sample, 50 mg) with a phosphate buffer (0.1 M, pH = 6.4) and then heating in a boiling-water bath with periodic shaking for 1 h [25]. The obtained supernatants and washed solution from the mixtures were added and diluted with distilled water to 100-mL volumetric flask. The absorbance of the solution was then measured at 565 nm by UV-vis spectrophotometry.

3. Results and discussion

3.1. Morphology structure

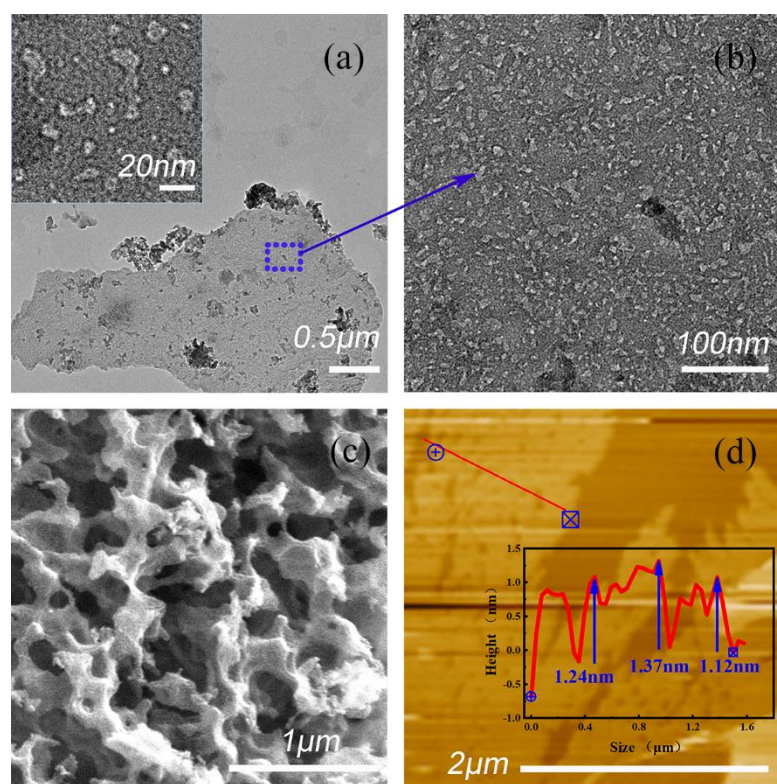


Fig. 1. (a, b) TEM, (c) SEM, and (d) AFM with corresponding cross-section profile of CN-PVP photocatalyst.

The morphology and structure of the as-prepared CN-PVP was studied by TEM and SEM. As shown in Fig. 1a, the CN-PVP possesses a clear ultrathin layer structure with a large amount of pores. In the TEM image with high magnification, a lot of worm-like porous structures can be observed (Fig. 1b). SEM image shows that the CN-PVP has sponge-like structure and consists of many curved nanosheets with lamellar morphology (Fig. 1c). Coupled with the AFM analysis in which the thickness of CN-PVP is less than 1.37 nm (Fig. 1d), it suggests that the number of layers in CN-PVP nanosheets are less than 3. Such ultrathin layer of nanosheets may cause an improved charge transfer in carbon nitride.

3.2. Crystal structure and Photocatalytic hydrogen evolution

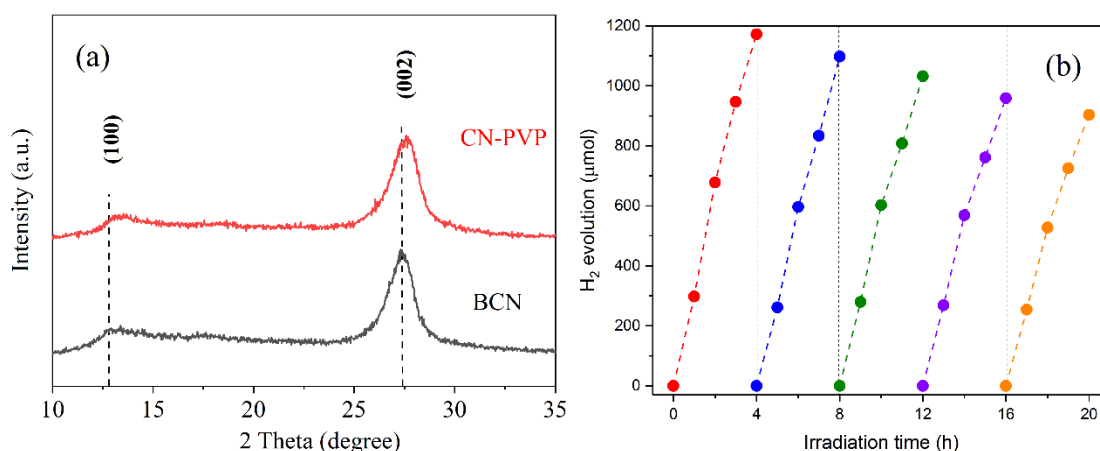


Fig. 2. (a) XRD patterns of CN-PVP and BCN; (b) repeated time courses of H₂ gas evolution over CN-PVP.

Fig. 2a displays the XRD patterns of BCN and CN-PVP samples. Both of them have two obvious characteristic peaks at about 12.6° and 27.3°, which are ascribed to (100) and (002) peaks according to JCPDS 87-1526, respectively [26]. Compared to BCN, the (002) peak is wider and shifts to higher angles in CN-PVP (from 27.3° in BCN to 27.6° in CN-PVP), which is ascribed to the formation of defects or porous structure [27,28]. The small diffraction peak at 12.6° in BCN corresponds to tri-s-triazine units, which shifts to 13.0° in CN-PVP also owing to the layered porous structure.

The photocatalytic water splitting reactions for hydrogen evolution on the as-prepared CN-PVP and BCN were carried out by using TEOA as electron donor and 1wt% of Pt as cocatalyst under white LED lamp irradiation. The photocatalytic performance is remarkably enhanced over CN-PVP sample. As shown in Fig. S6a and 2b, the evolved hydrogen amount in the initial one hour over CN-PVP is 297.6 μmol,

which is about 9.6 times higher than that of the BCN (31.2 μmol). The photocatalytic stability was also investigated through a cycling experiment. As shown in Fig. 2b, the high photocatalytic performance can be well maintained after five repeated experiments, indicating the high stability of photocatalytic hydrogen evolution. In addition, we found that CN-PVP sample also exhibits better ability than BCN for fixing nitrogen, indicating the advantage of CN-PVP (Fig. S6b).

3.3. Chemical structure

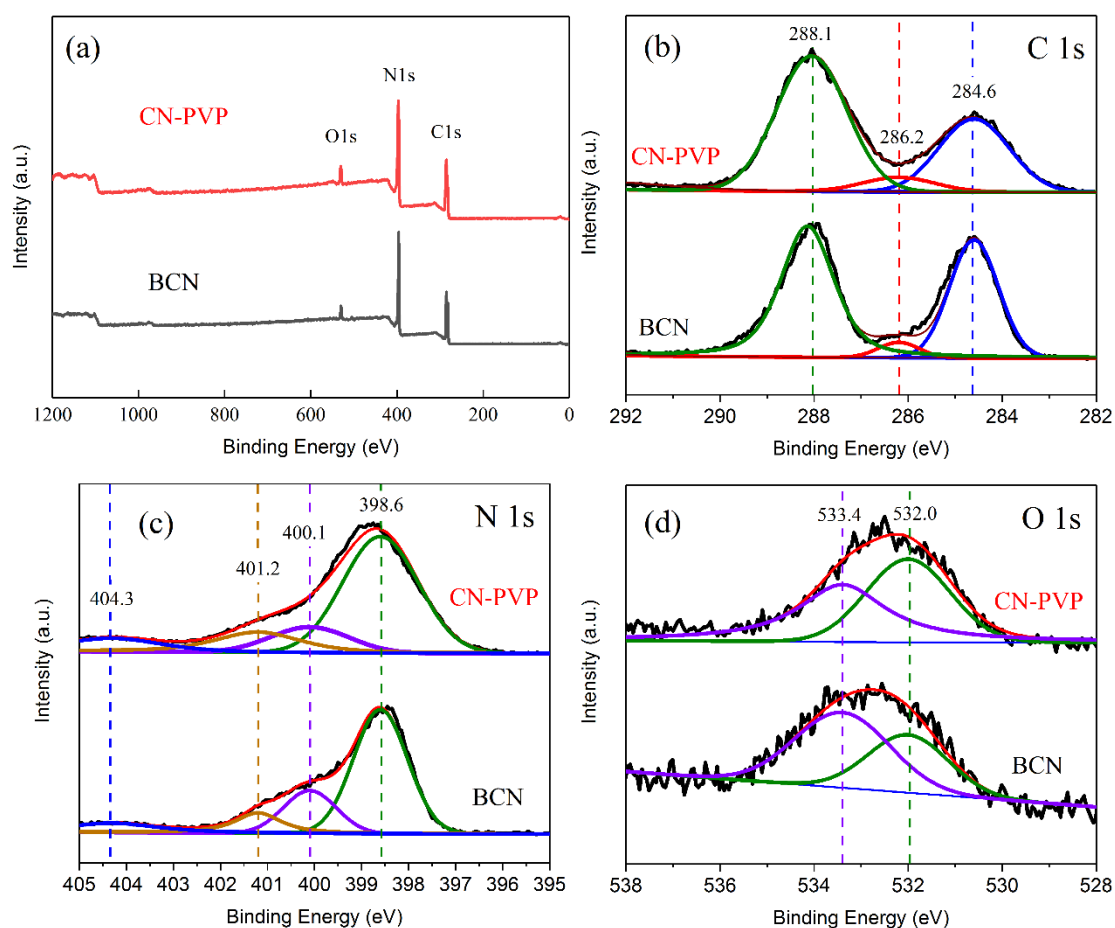


Fig. 3. XPS spectra of CN-PVP and BCN samples: (a) total survey, (b) C 1s, (c) N 1s and (d) O 1s.

The chemical states of samples were characterized by XPS measurement. As

shown in Fig. 3a, XPS survey spectra of both CN-PVP and BCN contain three sharp peaks at 288, 399, and 532 eV, which are respectively assigned to C 1s, N 1s, and O 1s signals. Thus, high resolution XPS spectra of C 1s, N 1s, and O 1s were recorded as shown in Fig. 3b-d, respectively. The C 1s spectra of BCN and CN-PVP are fitted with three peaks at 288.1, 286.2 and 284.6 eV, corresponding to the sp^2 -hybridized carbon in N containing aromatic ring, the sp^2 -bonded C atoms in the aromatic ring attached to the $-NH_x$ on the edges of tri-s-triazine units, and the C atoms in the sp^2 aromatic bonds, respectively [29]. It is obvious that the 284.6 eV peak content is much lower in CN-PVP than that in BCN. The decrease of C-C content suggests the deficiency of carbon atoms [30]. The N 1s spectra (Fig. 3c) could be deconvoluted into four components at 398.6, 400.1, 401.2, and 404.3 eV, ascribed to the sp^2 -bonded N in the tri-s-triazine units (N_{2C}), the bridging nitrogen atoms in $N-(C)_3$ (N_{3C}), the nitrogen atoms bonded with hydrogen atoms ($C-NH_x$) and the charging effects, respectively [31]. Compared with BCN, the peak area of N_{3C} decreases but that of $C-NH_x$ increases in CN-PVP. Notably, more amino nitrogen atoms are presented in CN-PVP than that in BCN. The increase of amino groups is also attributed to the disappearance of carbon atoms and the formation of carbon vacancies [32]. Moreover, it is clear that the intensities of C 1s and N 1s spectra of CN-PVP increase. The reason may be that C and N atoms neighboring carbon vacancies get fewer electrons than those on the normal sites [33]. In O 1s spectra the peaks appeared at 533.4 and 532.0 eV are assigned to the absorbed O_2 and H_2O on the surface of the samples [34].

Furthermore, the result of XPS analysis reveals that the C/N molar ratio in CN-

PVP (0.89) is much smaller than that in bulk one (1.08), indicating the formation of carbon vacancies. However, the result from combustion elemental analysis (Table S1) shows a different result that the C/N atomic ratio in CN-PVP (0.606) is larger than that in BCN (0.584), suggesting the presence of nitrogen vacancies. The creation of carbon vacancies may be attributed to the reaction between some carbon species and the pyrolysis-generated ammonia at high temperature [35]. Nitrogen vacancies might be result in the pyrolysis-generated template-producing atmosphere, which was consistent with the previous report that the N vacancy could be formed by the calcination under CO₂ [36]. The more NH_x/N-(C)₃ in CN-PVP contains more NH_x groups to promote the interaction between the layers through the hydrogen bonding [37]. It suggests that carbon atoms on the surface of sample escape quickly and left vacancies, while the pyrolysis of template will result in the nitrogen vacancies in CN-PVP, which will be supported by the following investigation results.

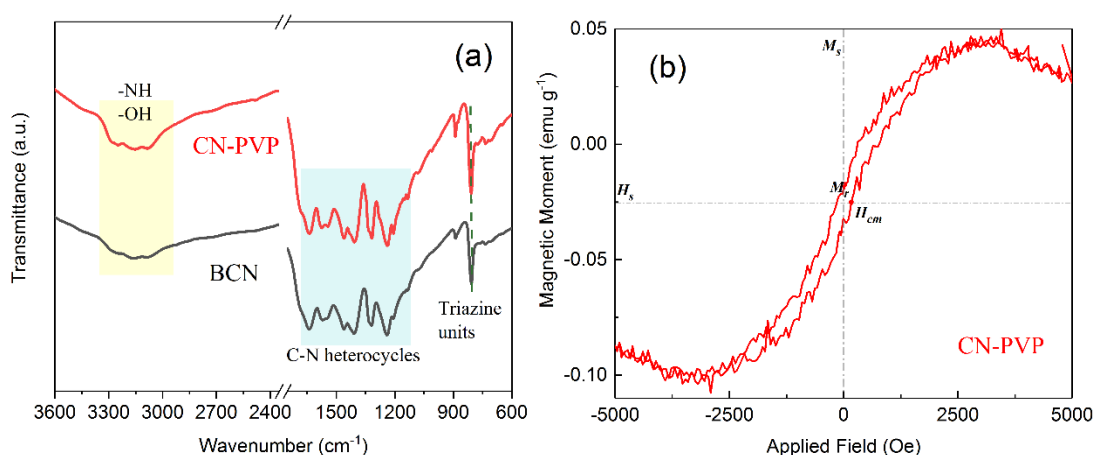


Fig. 4. (a) FT-IR spectra of CN-PVP and BCN and (b) VSM curve of CN-PVP.

Moreover, Fig. 4a presents FTIR spectra of both CN-PVP and BCN. It is obvious that two samples show the similar framework. The peaks centered at 811 and 887 cm⁻¹,

the regions in the range of 1200-1700 cm^{-1} and 2900-3600 cm^{-1} are ascribed to the breathing mode of triazine units, N-H bonds, stretching vibration modes of C-N heterocycles and surface amine groups/absorbed water molecules, respectively, indicating the original skeleton structure is essentially unchanged [38]. However, the intensity of 811 cm^{-1} peak increases in CN-PVP, suggesting that the integrity of conjugated structure is destroyed after defects generating [39]. Furthermore, the peaks at 3185-3261 cm^{-1} are attributed to terminal -NH and -NH₂ groups [40]. The peaks of -NH₂ for CN-PVP at 887 and 3185-3261 cm^{-1} are more intense compared with those for BCN, suggesting that more -NH₂ is generated in CN-PVP. It is believed that carbon nitride stripping and amino groups formation are accompanied by the generation of carbon vacancies [41-43]. Then, the -NH₂ groups of the carbon nitride structures are further measured by a ninhydrin test. The results are that the amino group densities in the CN-PVP and BCN are 12.91×10^{-5} and 5.68×10^{-5} mol g⁻¹, respectively. The high density of amino groups (-NH₂) formed in CN-PVP should be attributed to the disappearance of tertiary carbon, further confirming the formation of carbon vacancies [44]. Moreover, the result from the combustion elemental analysis shown in Table S1, showing that the C content in BCN is 34.9 % higher than that of CN-PVP (34.7 %). It suggests that carbon vacancies are formed in the CN-PVP layers. Meanwhile, the content of N in CN-PVP (57.4 %) is also lower than that in BCN (59.8 %), owing to the different formation processes involved.

The room temperature ferromagnetism in carbon nitride caused by spin-polarized conduction electrons in the spin-down branch is regarded as the result of carbon

vacancies induction [45]. Thus, in order to further confirm the existence of carbon vacancies, the magnetic measurement was carried out. As shown in Fig. 4b, the magnetization versus magnetic field (M-H) curve for the CN-PVP measured at 300 K shows an obvious hysteresis loop, confirming the room-temperature ferromagnetism of CN-PVP. In addition, the measured saturation magnetization and coercive force of CN-PVP are 0.047 emu g^{-1} and 200 Oe at 300 K respectively, much higher than those of the carbon nitride nanosheets with the thickness of about 2.6 nm in the previous literature (0.015 emu g^{-1} and 87 Oe) [46]. Ultrathin layered porous structures and carbon vacancies in CN-PVP can give more suspended hydrogen bonds, leading to the higher saturation magnetization.

3.4. Optical and electrochemical analysis

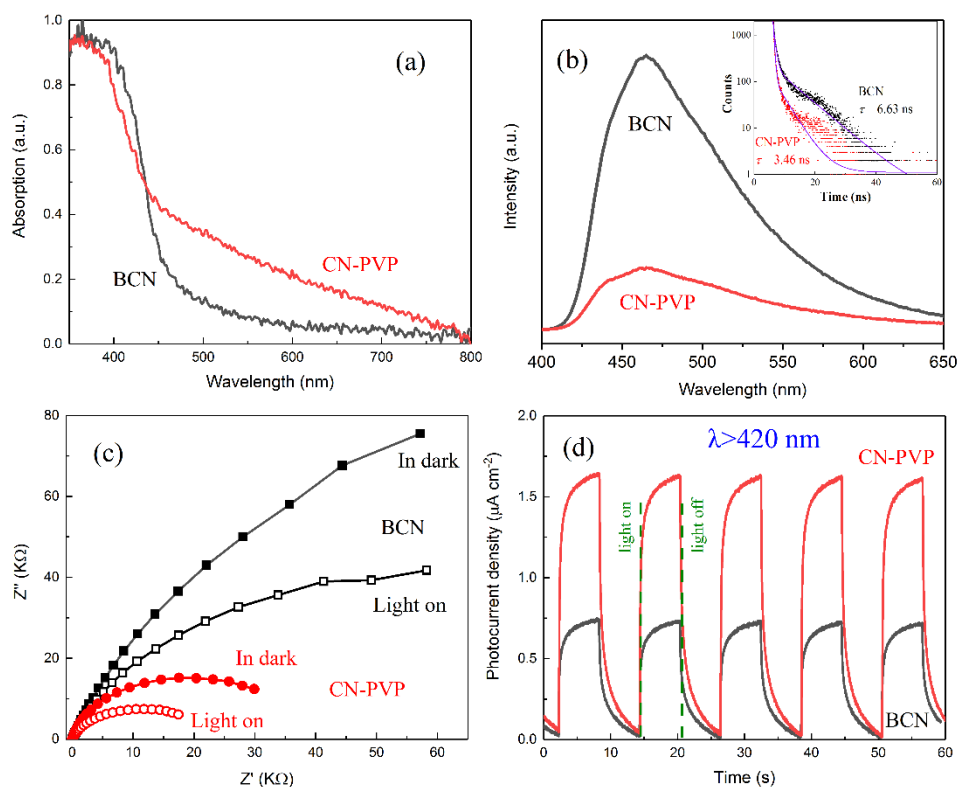


Fig. 5. (a) DRS, (b) PL and decay (insert), (c) EIS and (d) Photocurrent spectra of CN-PVP and BCN.

The unique holey nanosheet structure containing carbon and nitrogen vacancies has a large effect on the properties of CN-PVP. As shown in Fig. 5a, compared with the 450 nm (2.67 eV) in BCN, the absorption edge of CN-PVP is red shifted to 482 nm, corresponding to a band gap of 2.52 eV. Furthermore, a broader and stronger absorption tail, starting at 436 nm, is also clearly observed, which thus gives CN-PVP a beige color.

Then, PL spectra was measured to investigate the charge separation efficiency (Fig. 5b). The CN-PVP shows the same broad emission peak centered at 465 nm as BCN, owing to the delocalized π^* -n radiative transition [47]. Obviously, the peak intensity of CN-PVP is much lower than that of BCN, suggesting the improved charge separation. The PL lifetime of charge carriers was measured by the time-resolved PL spectra as shown in Fig. 5b (insert). It is clear that the average lifetime of CN-PVP (3.46 ns) is shorter than BCN (6.63 ns). It suggests that the energy relaxation is more likely to occur through nonradiative processes in CN-PVP, which will benefit for the photocatalytic hydrogen evolution.

Furthermore, electron paramagnetic resonance (EPR) analysis was performed to examine the electronic band structure and charge transfer in the photocatalysts, as shown in Fig. S7. The single EPR signal at 3502 G ($g=2.00276$) is observed for the two sample, which is related to the unpaired electrons originating from the odd numbers of carbon atoms in aromatic rings, indicating a well existent semiconductor framework [48]. CN-PVP exhibits much sharper signal than BCN, implying a greater ability for

generating delocalizing spins resulting in the higher charge transfer mobility.

In addition, it is clear that the EIS Nyquist plot arc radius of CN-PVP is smaller than that of BCN (Fig. 5c). Moreover, as shown in Fig. 5d, the photocurrent density of CN-PVP is higher than that of BCN, indicating that more efficient photoinduced electron-hole separation is achieved in CN-PVP, which gives support to the above analysis results.

3.5. Mechanism and AQY analysis

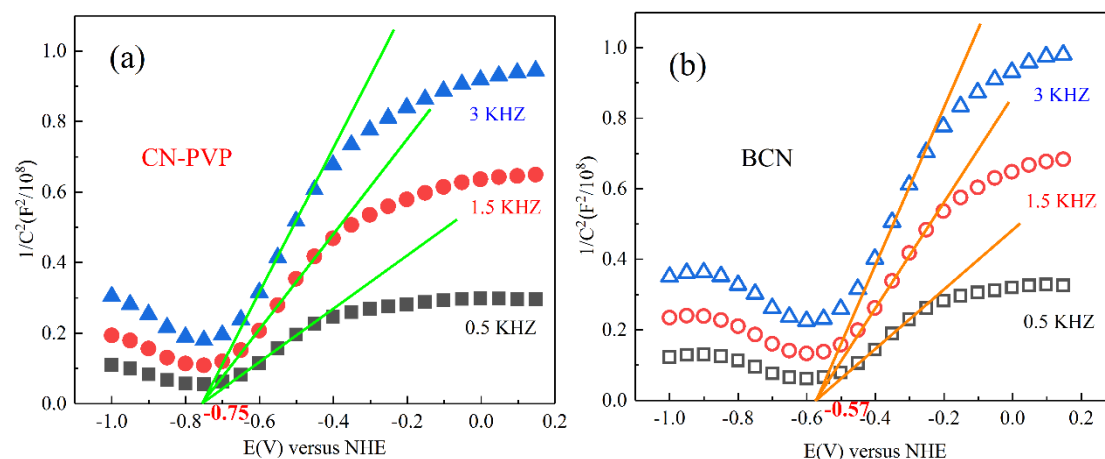


Fig. 6. Mott-Schottky plots of (a) CN-PVP and (b) BCN.

Additionally, the Mott-Schottky plots are employed to evaluate the flat band potentials of CN-PVP and BCN, which are separately deduced to be -0.75 and -0.57 V versus normal hydrogen electrode (NHE) as shown in Fig. 6a-b. Usually, the conduction band (CB) of one n-type semiconductor is thought to be about -0.2 V negative than the flat band potentials [49]. Thus, the CB values can be deduced to be -0.95 and -0.77 V for CN-PVP and BCN, respectively. Together with their bandgap values deduced from their UV-vis DRS absorption (Fig. 5a and s8), the relative energy levels of CN-PVP and

BCN are thus deduced and given in Fig. 7a. It is found that both CN-PVP and BCN satisfy the thermodynamical condition for photocatalytic hydrogen evolution. The band gap energy of CN-PVP is 2.52 eV smaller than that of BCN (2.67 eV), suggesting the enhanced light-harvesting capability of CN-PVP. In addition, new generated energy level, known as defect state, is also derived from UV-vis DRS (Fig. 5a and s8). Obviously, the potential of CB in CN-PVP occurs to negative shift compared to BCN, which is in favor of photocatalytic reductive reactions. Moreover, the newly formed defect states would act as donor level, enabling the absorption of photons with energies smaller than the band gap.

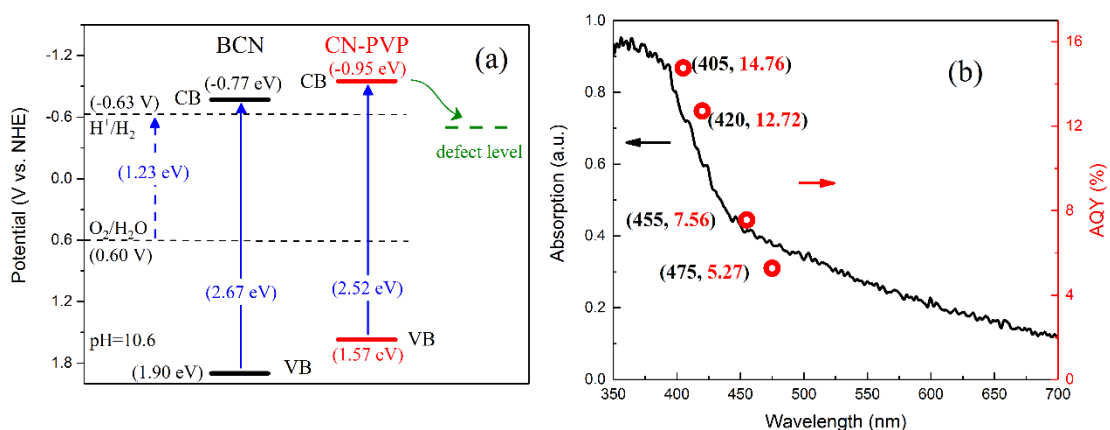


Fig. 7. (a) Electronic band structures of CN-PVP and BCN; (b) wavelength-dependent AQY of H₂ evolution over CN-PVP.

Considering that CN-PVP and BCN have similar chemical compositions, the unique porous structure with double heterogeneous vacancies provides more exposed active sites for the photocatalytic hydrogen evolution reaction. Furthermore, it is also beneficial for the rapid cross-plane diffusion of mass, photogenerated carriers, and hydrogen, which dramatically accelerate the photocatalytic reaction in kinetics [50]. Based on a combined analysis of DRS and the Mott-Schottky plots, CN-PVP can absorb

more visible light and have a more negative CB potential and a higher donor density, which promotes the photocatalytic reaction thermodynamically. Wavelength-dependent H_2 evolution of CN-PVP reveals that the variation tendencies of AQY dots coincided with its optical absorption spectrum indicating that the H_2 production is dominantly driven by photogenerated electrons (Fig. 7b). The AQY of CN-PVP at 420 nm is estimated to be about 12.7%, and the performance of CN-PVP is also higher than most of the existing carbon nitride based photocatalysts as summarized in Table S2.

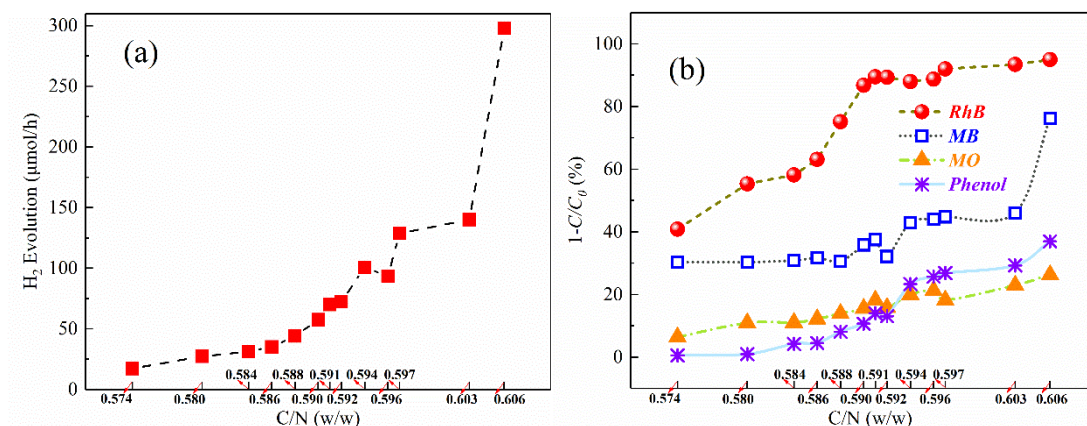


Fig. 8. (a) Hydrogen evolution rates for Pt-loaded photocatalysts with various mass ratio of carbon to nitrogen in TEOA aqueous solution; (b) different dyes degradation over carbon nitride with various mass ratio of carbon to nitrogen under white LED lamp irradiation.

The relationship between the photocatalytic performance and the C/N ratio of carbon nitride samples is summarized as shown in Fig. 8 and Table S3. It is clear that both the hydrogen evolution rate and dyes degradation ability increase with increasing the C/N ratio. The formation of vacancies can induce additional electron states below the conduction band, thus results in the narrowed bandgap and enhanced visible light absorption. Thus, such porous carbon nitride with double heterogeneous vacancies

shows excellent photocatalytic hydrogen evolution activity, owing to the promoted charge separation and more reaction sites.

4. Conclusion

In summary, using melamine as raw material and polyvinylpyrrolidone as template agent, the porous carbon nitride containing carbon and nitrogen vacancies was successfully prepared by simple thermal polymerization. The introduction of porous structure with double heterogeneous vacancies leads to a more efficient band gap for visible light collection and significantly increased charge transfer. Under white LED lamp irradiation, the hydrogen evolution rate of the porous carbon nitride is $297.6 \mu\text{mol h}^{-1}$, which is 9.6 times higher than that of the bulk one ($31.2 \mu\text{mol h}^{-1}$). This work provides a new idea for preparing porous carbon nitride with soft template.

CRedit authorship contribution statement

Huihui Li: Conceptualization, Methodology, Writing & review & editing, Software, Project administration, Funding acquisition, Supervision. **Fuchun Ning:** Data curation, Software. **Xiaofei Chen:** Validation. **Anye Shi:** Validation.

Declaration of Competing Interest

The authors declare that they have no known competing financial interests or personal relationships that could have appeared to influence the work reported in this paper.

Acknowledgment

This research was supported by the National Natural Science Foundation of China (51402139) and China Scholarship Council (201906185004).

Reference

- [1] T. Hisatomi, K. Domen, Reaction systems for solar hydrogen production via water splitting with particulate semiconductor photocatalysts, *Nat. Catal.*, 2 (2019) 387-399.
- [2] X. Wang, K. Maeda, A. Thomas, K. Takanabe, G. Xin, J. Carlsson, K. Domen, M. Antonietti, A metal-free polymeric photocatalyst for hydrogen production from water under visible light, *Nat. Mater.*, 8 (2009) 76-80.
- [3] Q. Han, B. Wang, J. Gao, L. Ou, Graphitic Carbon Nitride/Nitrogen-Rich Carbon Nanofibers: Highly Efficient Photocatalytic Hydrogen Evolution without Cocatalysts, *Angew. Chem. Int. Ed.*, 55 (2016) 10849-10853.
- [4] X. Lu, J. Xie, X. Chen, X. Li, Engineering MP_x ($M = Fe, Co$ or Ni) interface electron transfer channels for boosting photocatalytic H_2 evolution over $g-C_3N_4/MoS_2$ layered heterojunctions, *Appl. Catal. B*, 252 (2019) 250-259.
- [5] X. Wu, H. Ma, W. Zhong, J. Fan, H. Yu, Porous crystalline $g-C_3N_4$: Bifunctional $NaHCO_3$ template-mediated synthesis and improved photocatalytic H_2 -evolution rate, *Appl. Catal. B*, 271 (2020) 118899.
- [6] M. Zhou, G. Dong, F. Yu, Y. Huang, The deep oxidation of NO was realized by Sr multi-site doped $g-C_3N_4$ via photocatalytic method, *Appl. Catal. B*, 256 (2019) 117825.
- [7] R. Zhang, P. Li, F. Wang, L. Ye, A. Gaur, Z. Huang, Z. Zhao, Y. Bai, Y. Zhou, Atomically dispersed Mo atoms on amorphous $g-C_3N_4$ promotes visible-light absorption and charge carriers transfer, *Appl. Catal. B*, 250 (2019) 273-279.
- [8] J. Bai, L. Wang, Y. Zhang, C. Wen, X. Wang, H. Yang, Carboxyl functionalized graphite carbon nitride for remarkably enhanced photocatalytic hydrogen evolution,

Appl. Catal. B, 266 (2020) 118590.

[9] M. Zhang, J. Xu, R. Zong, Y. Zhu, Enhancement of visible light photocatalytic activities via porous structure of g-C₃N₄, Appl. Catal. B, 147 (2014) 229-235.

[10] Y. Li, Z. Ruan, Y. He, J. Li, K. Li, Y. Jiang, X. Xu, Y. Yuan, K. Lin, In situ fabrication of hierarchically porous g-C₃N₄ and understanding on its enhanced photocatalytic activity based on energy absorption, Appl. Catal. B, 236 (2018) 64-75.

[11] J. Jiang, X. Wang, Y. Liu, Y. Ma, T. Li, Y. Lin, T. Xie, S. Dong, Photo-Fenton degradation of emerging pollutants over Fe-POM nanoparticle/porous and ultrathin g-C₃N₄ nanosheet with rich nitrogen defect: Degradation mechanism, pathways, and products toxicity assessment, Appl. Catal. B, 278 (2020) 119349.

[12] Y. Zhang, S. Zong, C. Cheng, J. Shi, P. Guo, X. Guan, B. Luo, S. Shen, L. Guo, Rapid high-temperature treatment on graphitic carbon nitride for excellent photocatalytic H₂-evolution performance, Appl. Catal. B, 233 (2018) 80-87.

[13] D. Ruan, S. Kim, M. Fujitsuka, T. Majima, Defects rich g-C₃N₄ with mesoporous structure for efficient photocatalytic H₂ production under visible light irradiation, Appl. Catal. B, 238 (2018) 638-646.

[14] D. Zhang, Y. Guo, Z. Zhao, Porous defect-modified graphitic carbon nitride via a facile one-step approach with significantly enhanced photocatalytic hydrogen evolution under visible light irradiation, Appl. Catal. B, 226 (2018) 1-9.

[15] S. Bai, N. Zhang, C. Gao, Y. Xiong, Defect engineering in photocatalytic materials, Nano Energy, 53 (2018) 296-336.

[16] Q. Liang, Z. Li, Z. Huang, F. Kang, Q. Yang, Holey Graphitic Carbon Nitride

Nanosheets with Carbon Vacancies for Highly Improved Photocatalytic Hydrogen Production, *Adv. Funct. Mater.*, 25 (2015) 6885-6892.

[17] Y. Li, M. Gu, T. Shi, W. Cui, X. Zhang, F. Dong, J. Cheng, J. Fan, K. Lv, Carbon vacancy in C_3N_4 nanotube: Electronic structure, photocatalysis mechanism and highly enhanced activity, *Appl. Catal. B*, 262 (2020) 118281.

[18] P. Yang, J. Zhao, W. Qiao, L. Li, Z. Zhu, Ammonia-induced robust photocatalytic hydrogen evolution of graphitic carbon nitride, *Nanoscale*, 7 (2015) 18887-18890.

[19] S. Li, G. Dong, R. Hailili, L. Yang, Y. Li, F. Wang, Y. Zeng, C. Wang, Effective photocatalytic H_2O_2 production under visible light irradiation at g- C_3N_4 modulated by carbon vacancies, *Appl. Catal. B*, 190 (2016) 26-35.

[20] Y. Xie, Y. Li, Z. Huang, J. Zhang, X. Jia, X. Wang, J. Ye, Two types of cooperative nitrogen vacancies in polymeric carbon nitride for efficient solar-driven H_2O_2 evolution, *Appl. Catal. B*, 265 (2020) 118581.

[21] G. Xu, J. Shen, S. Chen, Y. Gao, H. Zhang, J. Zhang, Double Defects Modified Carbon Nitride Nanosheets with Enhanced Photocatalytic Hydrogen Evolution, *Phys. Chem. Chem. Phys.*, 20 (2018) 17471-17476.

[22] X. Wang, L. Wu, Z. Wang, H. Wu, X. Zhou, H. Ma, H. Zhong, Z. Xing, G. Cai, C. Jiang, F. Ren, C/N Vacancy Co-Enhanced Visible-Light-Driven Hydrogen Evolution of g- C_3N_4 Nanosheets Through Controlled He^+ Ion Irradiation, *Sol. RRL.*, 3 (2019) 1800298.

[23] Y. Yu, W. Yan, X. Wang, P. Li, W. Gao, H. Zou, S. Wu, K. Ding, Surface Engineering for Extremely Enhanced Charge Separation and Photocatalytic Hydrogen

Evolution on g-C₃N₄, *Adv. Mater.*, 30 (2018) 1705060.

[24] L. Lin, Z. Lin, J. Zhang, X. Cai, W. Lin, Z. Yu, X. Wang, Molecular-level insights on the reactive facet of carbon nitride single crystals photocatalysing overall water splitting, *Nat. Catal.*, 3 (2020) 649-655.

[25] G. Shiravand, A. Badiei, G. Ziarani, Carboxyl-rich g-C₃N₄ nanoparticles: synthesis, characterization and their application for selective fluorescence sensing of Hg²⁺ and Fe³⁺ in aqueous media, *Sensor. Actuat. B: Chem.*, 242 (2017) 244-252.

[26] F. Wang, Y. Wang, Y. Feng, Y. Zeng, Z. Xie, Q. Zhang, Y. Su, P. Chen, Y. Liu, K. Yao, W. Lv, G. Liu, Novel ternary photocatalyst of single atom-dispersed silver and carbon quantum dots co-loaded with ultrathin g-C₃N₄ for broad spectrum photocatalytic degradation of naproxen, *Appl. Catal. B*, 221 (2018) 510-520.

[27] J. Ding, W. Xu, H. Wan, D. Yuan, C. Chen, L. Wang, G. Guan, W. Dai, Nitrogen vacancy engineered graphitic C₃N₄-based polymers for photocatalytic oxidation of aromatic alcohols to aldehydes, *Appl. Catal. B*, 221 (2018) 626-634.

[28] J. Xiao, Y. Xie, F. Nawaz, Y. Wang, P. Du, H. Cao, Dramatic coupling of visible light with ozone on honeycomb-like porous g-C₃N₄ towards superior oxidation of water pollutants, *Appl. Catal. B*, 183 (2016) 417-425.

[29] M. Zhang, L. He, T. Shi, R. Zha, Neat 3D C₃N₄ monolithic aerogels embedded with carbon aerogels via ring-opening polymerization with high photoreactivity, *Appl. Catal. B*, 266 (2020) 118652.

[30] G. Dong, D. Jacobs, L. Zang, C. Wang, Carbon vacancy regulated photoreduction of NO to N₂ over ultrathin g-C₃N₄ nanosheets, *Appl. Catal. B*, 218 (2017) 515-524.

- [31] D. Zhu, Q. Zhou, Nitrogen doped g-C₃N₄ with the extremely narrow band gap for excellent photocatalytic activities under visible light, *Appl. Catal. B*, 281 (2021) 119474.
- [32] Z. Sun, W. Wang, Q. Chen, Y. Pu, H. He, W. Zhuang, J. He, L. Huang, A hierarchical carbon nitride tube with oxygen doping and carbon defects promotes solar-to-hydrogen conversion, *J. Mater. Chem. A*, 8 (2020) 3160.
- [33] S. Li, G. Dong, R. Hailili, L. Yang, Y. Li, F. Wang, Y. Zeng, C. Wang, Effective photocatalytic H₂O₂ production under visible light irradiation at g-C₃N₄ modulated by carbon vacancies, *Appl. Catal. B*, 190 (2016) 26-35.
- [34] C. Xu, S. Wu, G. Xiong, X. Guo, H. Yang, J. Yan, K. Cen, Z. Bo, K. Ostrikov, Nanoconfined fusion of g-C₃N₄ within edge-rich vertically oriented graphene hierarchical networks for high-performance photocatalytic hydrogen evolution utilizing superhydrophilic and superaerophobic responses in seawater, *Appl. Catal. B*, 280 (2021) 119461.
- [35] W. Luo, B. Wang, C. Heron, M. Allen, J. Morre, C. Maier, W. Stickle, X. Ji, Pyrolysis of cellulose under ammonia leads to nitrogen-doped nanoporous carbon generated through methane formation, *Nano Lett.*, 14 (2014) 2225
- [36] J. Xu, M. Fujitsuka, S. Kim, Z. Wang, T. Majima, Unprecedented effect of CO₂ calcination atmosphere on photocatalytic H₂ production activity from water using g-C₃N₄ synthesized from triazole polymerization, *Appl. Catal. B*, 241 (2019) 141-148.
- [37] X. Song, Q. Yang, X. Jiang, M. Yin, L. Zhou, Porous graphitic carbon nitride nanosheets prepared under self-producing atmosphere for highly improved

photocatalytic activity, *Appl. Catal. B*, 217 (2017) 322-330.

[38] S. Yang, Y. Gong, J. Zhang, L. Zhan, L. Ma, Z. Fang, R. Vajtai, X. Wang, P. Ajayan, Exfoliated Graphitic Carbon Nitride Nanosheets as Efficient Catalysts for Hydrogen Evolution Under Visible Light, *Adv. Mater.*, 25 (2013) 2452-2456.

[39] B. Wang, H. Cai, D. Zhao, M. Song, P. Guo, S. Shen, D. Li, S. Yang, Enhanced photocatalytic hydrogen evolution by partially replaced corner-site C atom with P in g-C₃N₄, *Appl. Catal. B*, 244 (2019) 486-493.

[40] A. Thomas, A. Fischer, F. Goettmann, M. Antonietti, J. Müller, R. Schlögl, J. Carlsson, Graphitic carbon nitride materials: variation of structure and morphology and their use as metal-free catalysts, *J. Mater. Chem.*, 18(2008) 4893-4908.

[41] K. Wang, J. Fu, Y. Zheng, Insights into photocatalytic CO₂ reduction on C₃N₄: Strategy of simultaneous B, K co-doping and enhancement by N vacancies, *Appl. Catal. B*, 254 (2019) 270-282.

[42] Z. Mo, X. Zhu, Z. Jiang, Y. Song, D. Liu, H. Li, X. Yang, Y. She, Y. Lei, S. Yuan, H. Li, L. Song, Q. Yan, H. Xu, Porous nitrogen-rich g-C₃N₄ nanotubes for efficient photocatalytic CO₂ reduction, *Appl. Catal. B*, 256 (2019) 117854.

[43] S. Guo, Y. Tang, Y. Xie, C. Tian, Q. Feng, W. Zhou, B. Jiang, P-doped tubular g-C₃N₄ with surface carbon defects: Universal synthesis and enhanced visible-light photocatalytic hydrogen production, *Appl. Catal. B*, 218 (2017) 664-671.

[44] S. Cao, B. Fan, Y. Feng, H. Chen, F. Jiang, X. Wang, Sulfur-doped g-C₃N₄ nanosheets with carbon vacancies: General synthesis and improved activity for simulated solar-light photocatalytic nitrogen fixation, *Chem. Eng. J.*, 353 (2018) 147-

156.

[45] D. Gao, Q. Xu, J. Zhang, Z. Yang, M. Si, Z. Yan, D. Xue, Defect-related ferromagnetism in ultrathin metal-free g-C₃N₄ nanosheets, *Nanoscale*, 6 (2014) 2577-2581.

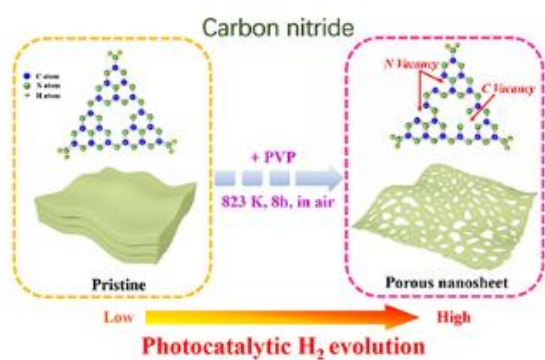
[46] K. Xu, X. Li, P. Chen, D. Zhou, C. Wu, Y. Guo, L. Zhang, J. Zhao, X. Wu, Y. Xie, Hydrogen dangling bonds induce ferromagnetism in two-dimensional metal-free graphitic-C₃N₄ nanosheets, *Chem. Sci.*, 6 (2015) 283-287.

[47] Y. Jing, Z. Sun, C. Tang, Y. Zhou, L. Zeng, L. Huang, Enhancement of photocatalytic hydrogen evolution activity of porous oxygen doped g-C₃N₄ with nitrogen defects induced by changing electron transition, *Appl. Catal. B*, 240 (2019) 30-38.

[48] S. Li, Y. Peng, C. Hu, Z. Chen, Self-assembled synthesis of benzene-ring-grafted g-C₃N₄ nanotubes for enhanced photocatalytic H₂ evolution, *Appl. Catal. B*, 279 (2020) 119401.

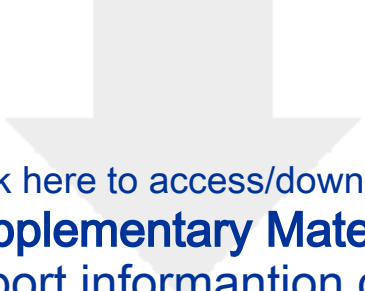
[49] K. Gelderman, L. Lee, S. Donne, Flat-Band Potential of a Semiconductor: Using the Mott–Schottky Equation, *J. Chem. Educ.* 84 (2007) 685.

[50] Y. Yin, J. Han, Y. Zhang, X. Zhang, P. Xu, Q. Yuan, L. Samad, X. Wang, Y. Wang, Z. Zhang, P. Zhang, X. Cao, B. Song, S. Jin, Contributions of Phase, Sulfur Vacancies, and Edges to the Hydrogen Evolution Reaction Catalytic Activity of Porous Molybdenum Disulfide Nanosheets, *J. Am. Chem. Soc.*, 138 (2016) 7965-7972.

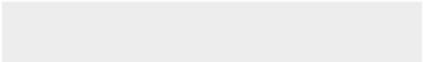



A proper PVP adding and heating in air realized pores formation and generated body defects in carbon nitride. Both carbon and nitrogen defects are formed. Benefiting from the synergy between carbon and nitrogen defects, such porous carbon nitride exhibits excellent photocatalytic hydrogen evolution performance. In addition, photocatalytic hydrogen evolution activity increases with increasing the carbon to nitrogen atomic ratio in carbon nitride.

- Carbon nitride porous nanosheets was prepared using melamine and PVP as precursors.
- Carbon vacancies were formed along with nitrogen vacancies.
- Porous nanosheets shows greatly improved photocatalytic H₂ evolution activity
- Photocatalytic performance is growing with the increase of C/N ratio.



Click here to access/download
Supplementary Material
support informantion.docx



Declaration of interest statement

We declare that we have no financial and personal relationships with other people or organizations that can inappropriately influence our work, there is no professional or other personal interest of any nature or kind in any product, service and/or company that could be construed as influencing the position presented in, or the review of, the manuscript entitled.